Journal of Materials Chemistry A

PAPER

View Article Online
View Journal | View Issue

Published on 10 December 2013. Downloaded by Michigan State University on 20/01/2016 21:24:40.

Cite this: J. Mater. Chem. A, 2014, 2, 2708

# One-pot sequential electrochemical deposition of multilayer poly(3,4-ethylenedioxythiophene):poly(4-styrenesulfonic acid)/tungsten trioxide hybrid films and their enhanced electrochromic properties†

Han Ling,[a] Jinlin Lu,[b] Silei Phua,[a] Hai Liu,[a] Liang Liu,[c] Yizhong Huang,[a] Daniel Mandler,[c] Pooi See Lee[ab] and Xuehong Lu*[ab]

Received 20th November 2013
Accepted 9th December 2013

DOI: 10.1039/c3ta14781a

www.rsc.org/MaterialsA

Hybrid thin films composed of multilayer poly(3,4-ethylenedioxythiophene):poly(4-styrenesulfonic acid) (PEDOT:PSS) and tungsten trioxide ($WO_3$) were electrochemically deposited on indium tin oxide (ITO) from a one-pot solution using a square-wave galvanostatic method. The morphology of the hybrid thin films could be easily manipulated to optimize their electrochromic properties by adjusting deposition conditions. In the hybrids, both components can be simultaneously switched to coloured or bleached states. The hybrid film obtained with very short deposition times of PEDOT:PSS and $WO_3$ in each cycle exhibits significantly enhanced electrochromic properties. The optical contrast of the hybrid film is higher than that of PEDOT:PSS or $WO_3$ films of the same thickness. Moreover, the stability of the hybrid film is also drastically enhanced. The enhancement may be attributed to the favourable interactions between the two components, *i.e.*, PEDOT:PSS may enter the defect sites in electrodeposited $WO_3$, preventing surface-defect-induced anodic dissolution during cycling, while the surface functional groups of $WO_3$ may act as dopants to inhibit over-oxidation of PEDOT, as well as the large interfacial area created using this unique one-pot multilayer deposition method.

## 1. Introduction

Electrochromism refers to the phenomenon of reversible colour change of materials induced by the application of an external electrical potential. Electrochromic materials have drawn increasing attention in recent years owing to their great potential in energy-saving smart windows, displays and some other applications.[1,2] Most electrochromic materials are redox active materials, of which the most widely studied ones are transition metal oxides (TMOs) and conjugated polymers.[2,3] Crystalline TMOs usually exhibit good chemical and thermal stabilities with slow switching speed.[2,4] By contrast, conjugated polymers have advantages in multicolouration, coloration efficiency and switching speed, whereas they suffer from poor stabilities.[3,5,6]

To overcome the problems associated with electrochromic TMOs and conjugated polymers, a popular approach is to synthesize TMO/conjugated polymer hybrid electrochromic materials as the structural and morphological modifications brought by the hybridization, especially the interfacial interactions between the two components, may lead to significant improvements in electrochromic properties of the hybrids. For example, Xiong *et al.* reported that in electrochromic polyaniline (PANI)/titanium oxide ($TiO_2$) hybrids with interfacial covalent bonds, significant electron donor (PANI)–acceptor ($TiO_2$) interactions could cause reduction in HOMO energy that enables PANI to be oxidized at a lower potential and hence leads to greatly improved electrochemical stability.[7] More recently, a hybrid system based on PANI/tungsten trioxide ($WO_3$) has been reported by J. Zhang *et al.*[8] The hybrids exhibit both long cycle life and fast switching speed as the interactions between PANI and $WO_3$ help to slow down the surface-defect-induced degradation of amorphous $WO_3$ and at the same time depress the over-oxidation of PANI.[8] In the aforementioned hybrid systems, the organic and inorganic components are, however, anodically and cathodically colouring materials, respectively. Thus, the optical contrast of such hybrids is mainly contributed by switching of one component to different redox states, whereas the redox reactions of the other component have to be

[a]School of Material Science and Engineering, Nanyang Technological University, 50 Nanyang Avenue, Singapore 639798. E-mail: assxhlu@ntu.edu.sg; Fax: +65 67909081
[b]Temasek Laboratories @ NTU, Nanyang Technological University, 9th Storey, BorderX Block, Research Techno Plaza, 50 Nanyang Drive, Singapore 637553
[c]Institute of Chemistry, the Hebrew University of Jerusalem, Jerusalem 91904, Israel

† Electronic supplementary information (ESI) available: Pictures of obtained thin films, XRD patterns, additional XPS survey spectra, plots of current density *versus* scan rate or square root of scan rate, optical contrast at a certain wavelength region, and coloration efficiency of certain samples. See DOI: 10.1039/c3ta14781a



This journal is © The Royal Society of Chemistry 2014

Published on 10 December 2013. Downloaded by Michigan State University on 20/01/2016 21:24:40.

eliminated by controlling potentials in order to avoid their negative effect on optical contrast, *i.e.*, the second component does not act as an electrochromic material effectively.

To address the above issue, hybrid systems based on poly(3,4-ethylenedioxythiophene):poly(4-styrenesulfonic acid) (PEDOT:PSS) and $WO_3$, where both components are cathodically colouring materials, have attracted considerable attention. $WO_3$ is the most widely studied electrochromic TMO, which has been used as an electrochromic material in commercially available smart windows owing to its excellent electrochemical stability and relatively high coloration efficiency in comparison with those of other TMOs.[2,9] $WO_3$ turns from transparent to blue in the reduction process, which is caused by the reduction of $W^{VI}$ accompanied by the intercalation of small counter cations ($M^+$), such as $H^+$, $Li^+$, or $Na^+$, as shown in eqn (1).[10]

$$W^{VI}O_3 + xM^+ + xe^- \rightarrow M_xW_{(1-x)}{}^{VI}W_x{}^{V}O_3 \quad (1)$$

PEDOT:PSS is one of the most popular cathodically colouring conjugated polymers with high optical contrast, high coloration efficiency and fast switching speed, which turns from light blue to dark blue upon reduction.[11,12] The hybrid systems composed of these two components have been prepared and studied by several research groups.[13,14] Deepa *et al.* prepared a two-layer hybrid film composed of $WO_3$ and PEDOT:PSS by surfactant-mediated electrochemical deposition of $WO_3$ followed by spin coating of PEDOT:PSS and demonstrated enhanced long term stability of the film.[13] PEDOT:PSS/$WO_3$ hybrid films could also be fabricated from a solution containing 3,4-ethylenedioxythiophene (EDOT) and sodium tungstate dehydrate ($Na_2WO_4 \cdot 2H_2O$) by voltammetric potential cycling.[14] However, it remained a challenge to establish a simple synthesis method that allows tailoring of the hybrid structures at the nanometer scale so as to optimize the electrochromic properties of the hybrids.

In this article, we report a novel multilayer PEDOT:PSS/$WO_3$ hybrid system prepared by one-pot sequential electrochemical deposition. This facile method allows us to control the morphology by adjusting the deposition time for each layer, and hence the interfacial area and resultant electrochromic properties of the hybrids can be easily optimized. Herein, we demonstrate that by optimizing the morphology, both components in the hybrids can be simultaneously switched to a coloured or bleached state, giving rise to high optical contrast, while the cycle life of the hybrid greatly benefits from the interfacial interactions and large interfacial area created using such a one-pot sequential deposition method.

## 2. Experimental

### 2.1. Materials

All chemicals used in this work were purchased from Sigma-Aldrich and used as received. Unless specified, all experiments were conducted under ambient conditions and all solutions were prepared using de-ionized (DI) water. All electrodeposition/electropolymerization experiments were performed using a three-electrode system. Silicon dioxide-passivated, indium tin oxide-coated glass (ITO glass) with a sheet resistance $R_s = 5$–$15$ Ω and dimensions of $7 \times 50 \times 0.7$ mm (Delta Technologies, USA) was used as the working electrode. Before any deposition, the ITO glass was sonicated in acetone, isopropanol, ethanol and DI water for 5 minutes, respectively, and then blow-dried with nitrogen gas. A platinum (Pt) sheet with the dimension of $1 \times 2$ cm was used as the counter electrode. The reference electrode used was silver/silver chloride (Ag/AgCl in sat. KCl).

### 2.2. Preparation of electrochromic thin films

Appropriate solutions were first prepared for electrodeposition of PEDOT:PSS, $WO_3$ and PEDOT:PSS/$WO_3$ hybrid thin films on ITO glass substrates, respectively. For PEDOT:PSS films, a solution containing 0.02 mol $L^{-1}$ EDOT and a certain amount of poly(4-styrenesulfonic acid) (PSS) (weight ratio EDOT : PSS = 1 : 1.6) was electropolymerized at the current density of +0.5 mA $cm^{-2}$ for 50 seconds.[15] For $WO_3$ synthesis, 0.9 g tungsten (W) powder was dissolved in 30 mL of a 30 wt% $H_2O_2$ aqueous solution and the solution was refluxed at 60 °C until W powders were completely oxidized, giving a peroxotungstic acid (PTA) solution.[16,17] Excess $H_2O_2$ in the solution was removed by Pt black, and then 70 mL DI water was added to dilute the solution to achieve a PTA concentration of 0.05 mol $L^{-1}$. The $WO_3$ films were obtained by applying a current density of −0.6 mA $cm^{-2}$ to the working electrode for about 500 s. To prepare the hybrid thin films, EDOT and PSS were added into the PTA solution to achieve a solution with 0.02 mol $L^{-1}$ EDOT:PSS and 0.05 mol $L^{-1}$ PTA. The pH of the resultant solution is around 1.5–2.0. The hybrid thin films were then deposited using a galvanostatic square wave method. For example, in a typical process, a positive current density of +0.5 mA $cm^{-2}$ and a negative current density of −0.6 mA $cm^{-2}$ were alternately applied for 10 s and 60 s, respectively, to the working electrode for 5 cycles. The deposition area of all films is about 2 $cm^2$. The obtained films were rinsed with DI water and blow dried with nitrogen gas.

### 2.3. Characterization

The film thickness was measured using an Alpha-step 500 profilometer. A transmission electron microscope (TEM JEOL 2100F) equipped with an energy dispersive X-ray spectrometer (EDS) system was used to examine the cross-section of the electrochromic films. A field-effect scanning electron microscope (FESEM JEOL 6340F) was employed to examine the surface morphology of the films. The chemical structure and compositions of the thin films were characterized using Fourier transform infrared (FTIR) spectroscopy (Perkin Elmer Spectrum GX), X-ray photoelectron spectroscopy (XPS, Theta-probe, Thermo Scientific) and Raman spectroscopy (Witec confocal Raman spectrometer with an excitation light of 488 nm). The FTIR scan was conducted on a diamond attenuated total reflection (ATR) unit (Graseby Specac ATR10500) from 4000 to 600 $cm^{-1}$, with 16 scans collected for signal averaging. To compensate the surface-charging effects in XPS scans, the binding energy level of C1s was set at 285 eV for further data analysis. An X-ray diffraction spectrometer (Shimadzu) with Cu

Published on 10 December 2013. Downloaded by Michigan State University on 20/01/2016 21:24:40.

Kα radiation was used to identify the crystalline structure of $WO_3$ and hybrid thin films.

Cyclic voltammetry (CV) was measured using a multichannel AC/DC electrochemical impedance test station (Solartron Model 1470E) in 0.1 mol $L^{-1}$ lithium perchlorate ($LiClO_4$)/propylene carbonate (PC) solution. It was performed at scan rates of 5, 15, 25, 50, and 100 mV $s^{-1}$ within a potential range of [−1.0 to 1.0] V. The spectro-electrochemical properties of the films were measured using a Solartron Model 1470E and a UV-Vis-NIR spectrophotometer (Shimadzu UV 3600). The UV-Vis spectra of the thin films were recorded in the wavelength range of 300 nm to 800 nm at potentials of −1.0, 0, and 0.8 V. For each thin film, dynamic optical transmittance was also recorded at the wavelength of interest under a square wave potential oscillating between +0.8 V and −1.0 V at a time step of 50 s. The coloration efficiencies and switching times of the electrochromic thin films were measured according to the methods reported by Lu *et al.*[18]

# 3. Results and discussion

## 3.1. One-pot sequential electrochemical deposition of multilayer films

In this work, the constant-current-density electrodeposition method was used for one-pot sequential deposition of multilayer $WO_3$ and PEDOT:PSS thin films. The electropolymerization of EDOT:PSS occurred at the positive current,[15] while the electrodeposition of $WO_3$ is driven by electroreduction at negative potentials.[16,17,19] For the hybrid films, the two components were co-deposited from the same aqueous solution. Firstly, EDOT:PSS underwent oxidation electrochemical polymerization to form a PEDOT:PSS layer on ITO glass under positive current, and then PTA was reduced under negative current to form a $WO_3$ layer on top of the PEDOT:PSS layer; the reduction process may be accompanied by dehydration of the $WO_3$ layer as the reaction medium was highly acidic. The two layers together are defined as a bilayer in this paper. The process was repeated several times to achieve a multilayer hybrid thin film (Scheme 1).

Both neat $WO_3$ and PEDOT:PSS films show approximate linear relationships between the film thickness and deposition time (Fig. 1a and b), while the electrodeposition of $WO_3$ is much slower than the electropolymerization of EDOT. For the deposition of PEDOT:PSS/$WO_3$, the growth curve is also approximately linear (Fig. 1c). In this work, unless specified, the hybrid films used for property characterization all have 5 bilayers with an overall thickness of about 200 nm. $WO_3$ and PEDOT:PSS thin films of the same thickness were also fabricated as reference samples. Pictures of the as-deposited PEDOT:PSS, $WO_3$ and hybrid thin films on ITO glass are shown in the ESI (*cf.* Fig. S1†).

## 3.2. Morphologies of the hybrid thin films

To directly demonstrate the capability of this one-pot method for fabrication of multilayer PEDOT:PSS/$WO_3$ hybrid thin films, a TEM image of a hybrid thin film with relatively thick $WO_3$ and PEDOT:PSS layers is shown in Fig. 2. This hybrid thin film was deposited by applying 30 s of positive current density and 300 s of negative current density repeatedly. It can be seen that there are alternating dark and light layers. Within each bilayer, the dark region should be $WO_3$ or $WO_3$-rich region owing to the high atomic mass of W. It can also be observed that when a $WO_3$ layer is added onto a PEDOT:PSS layer, there is no clear boundary between the two layers, *i.e.*, the dark shade increases gradually. The likely reason for this is that upon applying the negative potential, the PEDOT:PSS layer may be reduced first. At the same time, the PTA ions may be attracted by the PSS anions in the partially reduced PEDOT:PSS to diffuse into PEDOT:PSS, since the PEDOT:PSS layer still has some conductivity, which may act as a porous electrode for the deposition of $WO_3$ inside the PEDOT:PSS layer, especially in the near surface region. Only

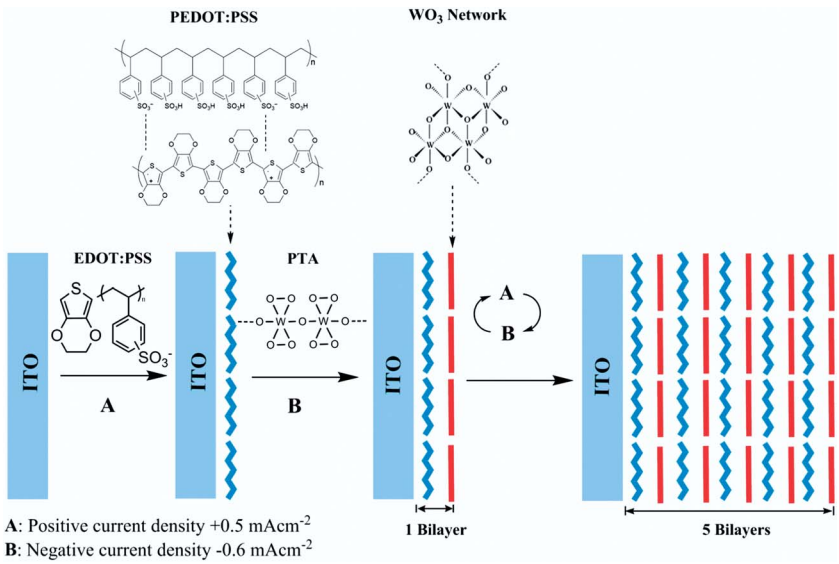


Scheme 1 Synthesis process for multilayer PEDOT:PSS/$WO_3$ hybrid thin films.

 This journal is © The Royal Society of Chemistry 2014

Published on 10 December 2013. Downloaded by Michigan State University on 20/01/2016 21:24:40.

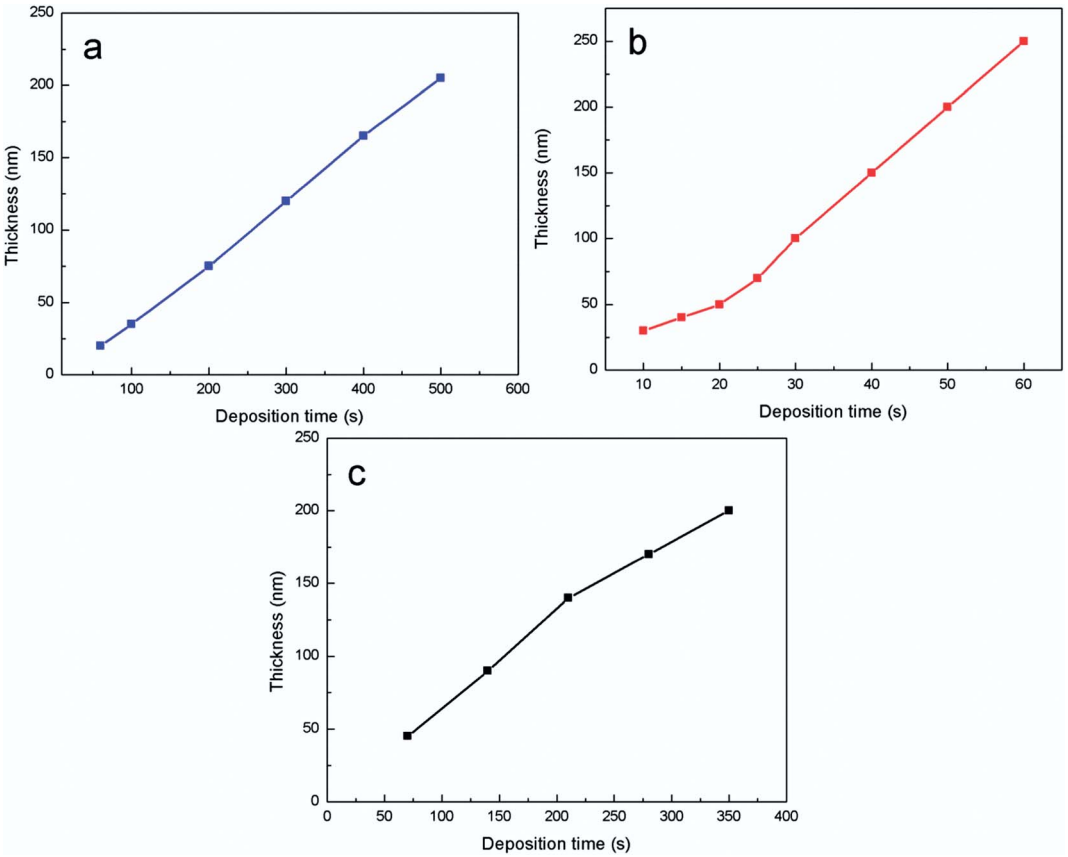


Fig. 1 Thickness of (a) $WO_3$, (b) PEDOT:PSS, and (c) hybrid films as a function of total deposition time.

after PEDOT:PSS is fully reduced or the PTA ions could not diffuse into the PEDOT:SS layer anymore, a neat $WO_3$ layer would form. On the other hand, when it is switched to the positive potential, $WO_3$, which has much lower electrical conductivity than PEDOT:PSS, would be oxidized and become more insulating. Hence, the oxidization of EDOT would not occur in the partially oxidized $WO_3$ layer significantly due to the very low conductivity inside, whereas the electropolymerization of EDOT:PSS would still occur on the surface of the $WO_3$ layer to some extent and once some conductive PEDOT:PSS species are formed on the surface, a layer of PEDOT:PSS would quickly form. Thus a sharp boundary appears when a PEDOT:PSS layer is added onto a $WO_3$ layer.

A unique advantage of this one-pot multilayer deposition method is that the morphology of the hybrid thin films can be facilely manipulated by controlling the deposition time for each layer. By shortening the deposition times, the layer thickness of both PEDOT:PSS and $WO_3$ could be reduced substantially to cause PEDOT:PSS and $WO_3$ interpenetrating each other, resulting in "layerless" morphology. The morphology of a "layerless" hybrid film fabricated by applying alternating positive current for 10 s and negative current for 60 s was examined using FESEM to compare with those of neat $WO_3$ and PEDOT:PSS films. As shown in Fig. 3a and b, both neat $WO_3$ and PEDOT:PSS films have relatively compact and smooth surfaces. However, when $WO_3$ is deposited on PEDOT:PSS (for 60 s only), the PEDOT:PSS/$WO_3$ film exhibits a loosely packed surface morphology (Fig. 3c); the discrete nanoparticles on the surface are likely to be $WO_3$ particles with PEDOT:PSS underneath. When PEDOT:PSS is deposited on PEDOT:PSS/$WO_3$ (for 10 s only), the PEDOT:PSS/$WO_3$/PEDOT:PSS film shows a very uneven surface morphology (Fig. 3d), implying that the surface may not be fully covered by a PEDOT:PSS layer. By repeating such short-time deposition, a "layerless" morphology would be formed. In later sections, the electrochemical and electrochromic properties presented are all based on the hybrid film with such a "layerless" morphology as it provides much larger interfacial area, benefiting electrochromic properties.

### 3.3. Structural verification

Chemical structures of the hybrid films are verified by ATR-FTIR spectroscopy. Fig. 4a shows the spectrum of the hybrid film with 5 bilayers in comparison with those of $WO_3$ and PEDOT:PSS reference films. From the $WO_3$ reference sample, two strong bands at 969 and 916 $cm^{-1}$ are observed, which can be attributed to asymmetric stretching vibrations of W=O double bonds of the amorphous $WO_3$ network.[8,20] While, the PEDOT:PSS reference sample exhibits bands at 1513 and 1310 $cm^{-1}$, which are attributed to the stretching of C=C and C–C bonds in the thiophene rings. The vibration of the C–S bond can also be observed at 685 $cm^{-1}$ and stretching of the ethylenedioxy group

Published on 10 December 2013. Downloaded by Michigan State University on 20/01/2016 21:24:40.

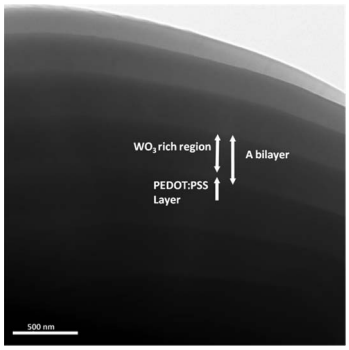


Fig. 2 A TEM micrograph showing a multilayer morphology of the hybrid thin film produced by altering deposition times for each component.

at 1083 $cm^{-1}$.[21,22] The hybrid film clearly exhibits the characteristic bands of both $WO_3$ and PEDOT:PSS, proving the existence of both components. To further confirm the multilayer structure, ATR-FTIR measurements were also carried out on the hybrid films with different numbers of layers, namely PEDOT:PSS, PEDOT:PSS/$WO_3$ ($WO_3$ on top), PEDOT:PSS/$WO_3$/PEDOT:PSS (PEDOT:PSS on top), and PEDOT:PSS/$WO_3$/PEDOT:PSS/$WO_3$ ($WO_3$ on top), respectively (Fig. 4b). In the hybrid thin films of PEDOT:PSS and PEDOT:PSS/$WO_3$/PEDOT:PSS, indeed the characteristic bands of PEDOT:PSS can be clearly observed, whereas the bands corresponding to $WO_3$ are relatively weak. By contrast, the spectra of the PEDOT:PSS/$WO_3$ and PEDOT:PSS/$WO_3$/PEDOT:PSS/$WO_3$ thin films exhibit relatively strong characteristic bands of both PEDOT:PSS and $WO_3$, implying that when switched to the negative current, a significant portion of $WO_3$ is formed inside of the PEDOT:PSS layer. This is consistent with the TEM result shown in the previous section (Fig. 2).

To further confirm the structure of the electrodeposited $WO_3$ layer, Raman spectroscopy and X-ray diffraction studies were conducted. Fig. 4c shows that the electrodeposited $WO_3$ film has two distinct Raman bands at 780 and 945 $cm^{-1}$. The band at around 780 $cm^{-1}$ can be attributed to $W^{VI}$–O bonds, while the one located at 945 $cm^{-1}$ can be assigned to the stretching of the terminal oxygen atoms in $W^{VI}$═O on the surface of the thin films.[23,24] In addition to the two strong Raman bands, a relatively weak Raman band is also noticeable at 620 $cm^{-1}$, which corresponds to the symmetric stretching mode of $W^{VI}(O_2)$, indicating that the reduction of peroxotungstates to $WO_3$ is not fully completed in the deposition process.[25] Moreover, the X-ray diffraction pattern shown in the ESI (*cf.* Fig. S2†) confirms that the electrodeposited $WO_3$ and hybrid thin films are both amorphous in nature.

XPS is used to further confirm the chemical structures of the hybrid films and probe interfacial interactions. Fig. 5a shows XPS spectra for W4f and S2p peaks of the hybrid thin films with the corresponding spectra of PEDOT:PSS and $WO_3$ films as references. The full XPS survey of the hybrid thin films with different numbers of layers is provided in the ESI (*cf.* Fig. S3†). For the neat $WO_3$ film, the two characteristic peaks at binding energies of 37.9 eV ($W4f_{7/2}$) and 35.7 eV ($W4f_{5/2}$) correspond to the oxidation state of $W^{VI}$,[16,23] indicating that W is at its highest oxidation state. The single-layer PEDOT:PSS thin film exhibits no characteristic W4f peaks. When a layer of $WO_3$ is deposited on top of the PEDOT:PSS layer, the PEDOT:PSS/$WO_3$ hybrid thin film shows two characteristic peaks at 38.2 eV ($W4f_{7/2}$) and 36.0 eV ($W4f_{5/2}$) respectively, which are 0.3 eV higher than that of the neat $WO_3$ film. The up-shift in binding energy is likely to

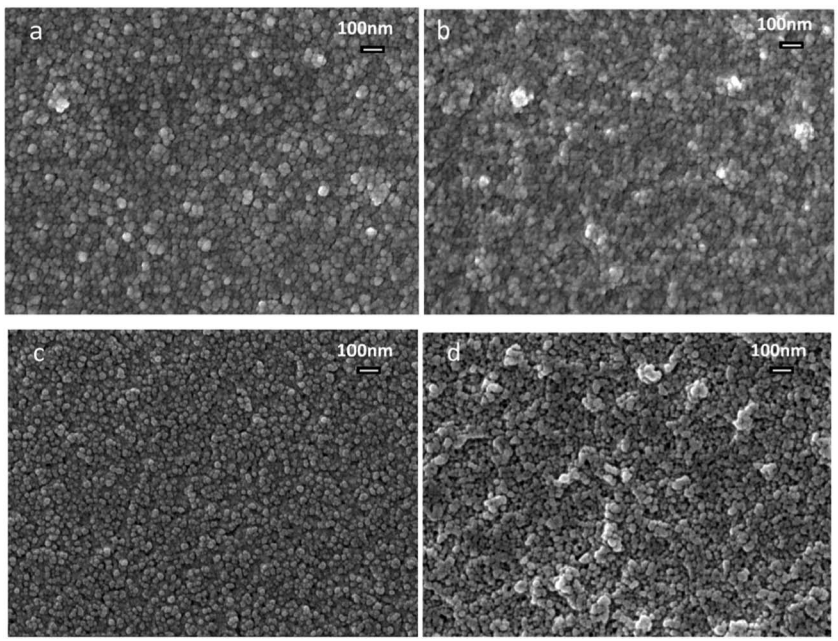


Fig. 3 FESEM micrographs showing surface morphologies of (a) neat $WO_3$, (b) neat PEDOT:PSS, (c) PEDOT:PSS/$WO_3$ and (d) PEDOT:PSS/$WO_3$/PEDOT:PSS films of the hybrid films.

 This journal is © The Royal Society of Chemistry 2014

Published on 10 December 2013. Downloaded by Michigan State University on 20/01/2016 21:24:40.

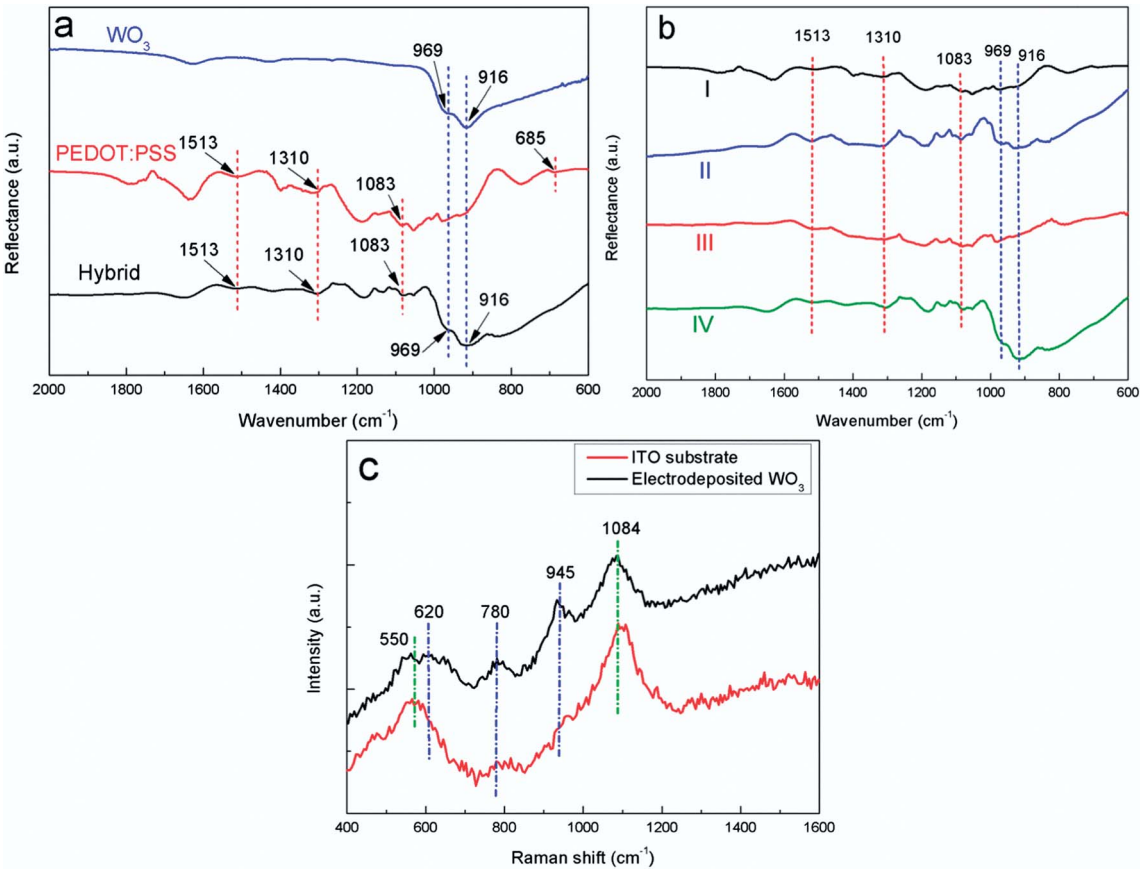


Fig. 4 ATR-FTIR spectra of (a) $WO_3$, PEDOT:PSS and the 5-bilayer hybrid thin film, and (b) the hybrid thin films with different number of layers: PEDOT:PSS (I), PEDOT:PSS/$WO_3$ (II), PEDOT:PSS/$WO_3$/PEDOT:PSS (III), PEDOT:PSS/$WO_3$/PEDOT:PSS/$WO_3$ (IV); (c) Raman spectra of ITO glass and the electrodeposited $WO_3$ thin film.

be associated with the presence of a large amount of defects, which are mainly caused by the incomplete reduction of peroxotungstates and –OH groups on the surface.[26] It is striking to see that in the spectrum of the PEDOT:PSS/$WO_3$/PEDOT:PSS hybrid film that has PEDOT:PSS as the top layer, although the intensities of the W4f peaks become lower owing to the coverage by PEDOT:PSS, the binding energies of the W4f peaks shift back to the positions for neat $WO_3$. This implies that driven by the anodic potential, EDOT molecules may be able to diffuse into the defect sites to form PEDOT:PSS. The PEDOT may interact with the defects in the $WO_3$ layer to reduce the electron withdrawing effect of the peroxide groups. Fig. 5b shows that the neat PEDOT:PSS thin film exhibits characteristic S2p peaks for two types of distinctly different sulphur (S) atoms; the broad

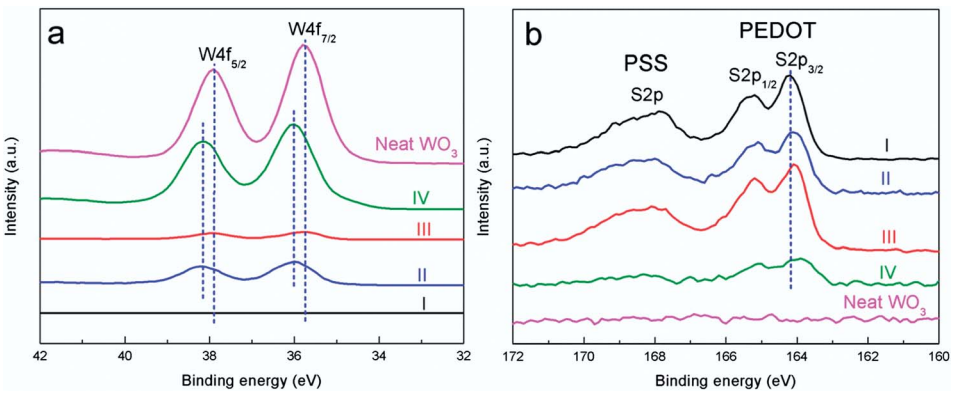


Fig. 5 XPS spectra in (a) W4f and (b) S2p region for neat PEDOT:PSS (I), PEDOT:PSS/$WO_3$ (II), PEDOT:PSS/$WO_3$/PEDOT:PSS (III), PEDOT:PSS/$WO_3$/PEDOT:PSS/$WO_3$ (IV) and neat $WO_3$ thin film.

Published on 10 December 2013. Downloaded by Michigan State University on 20/01/2016 21:24:40.

peak with higher binding energy can be attributed to the overlap of $S2p_{3/2}$ and $S2p_{1/2}$ peaks of the S atoms in PSS, while the duplet at a lower banding energy is from the S atoms in PEDOT.[21,27] In comparison with neat PEDOT:PSS, the hybrid films all exhibit slightly lower binding energies for the S2p peaks of PEDOT, implying that there may be some interactions between $WO_3$ defect sites and PEDOT. Such interactions may play important roles in influencing the electrochromic properties of the hybrids, which will be discussed in Section 3.5.

### 3.4. Electrochemical behaviour of the hybrid thin film

To understand the electrochemical behaviour of the hybrid films, three-electrode CV tests were conducted for $WO_3$, PEDOT:PSS and 5 bilayer hybrid thin films in a 0.1 mol $L^{-1}$ $LiClO_4$/PC solution, and the CV curves at various scan rates are shown in Fig. 6. In the scan rate range of 5 to 100 mV $s^{-1}$, $WO_3$ shows an obvious oxidation peak (Fig. 6a), while PEDOT:PSS shows a couple of redox peaks (Fig. 6b). The shape of the CV curves of the hybrid film in general is similar to that of $WO_3$ at relatively high scan rates, while distinct PEDOT:PSS redox peaks can be observed at relatively low scan rates (Fig. 6c). It suggests that both components in the hybrid film are electrochemically active. Thus, both components can be switched simultaneously to a coloured/bleached state under negative/positive potentials. The area enclosed by the CV curves quantifies the inserted and extracted charges. Comparing the CV curves of the three films at the scan rate of 100 mV $s^{-1}$, the hybrid film has the largest enclosed area, suggesting that more active units in the hybrid can be effectively oxidized/reduced probably because the PEDOT:PSS layer facilitates charge transfer,[28] making charge insertion/extraction into/from $WO_3$ easier. Indeed when the peak current densities for the anodic and cathodic peaks of the hybrid are plotted against the scan rate, $\nu$, approximate linear relationships are obtained, whereas the peak current densities have non-linear relationships with the square root of the scan rate, $\nu^{1/2}$ (Fig. S4†).[28] This signifies that both the oxidation and reduction in the hybrid are non-diffusion-controlled processes in the studied scan rate range.[29,30]

### 3.5. Electrochromic properties of the hybrid thin film

To characterize their electrochromic properties, all the films were tested in a three-electrode electrochemical cell with 0.1 mol $L^{-1}$ $LiClO_4$/PC solution as the electrolyte. With applied potentials from +0.8 V to −1.0 V, $WO_3$ changes from transparent to blue, PEDOT:PSS changes from pale blue to dark blue, while the hybrid changes from pale blue to grey blue. The

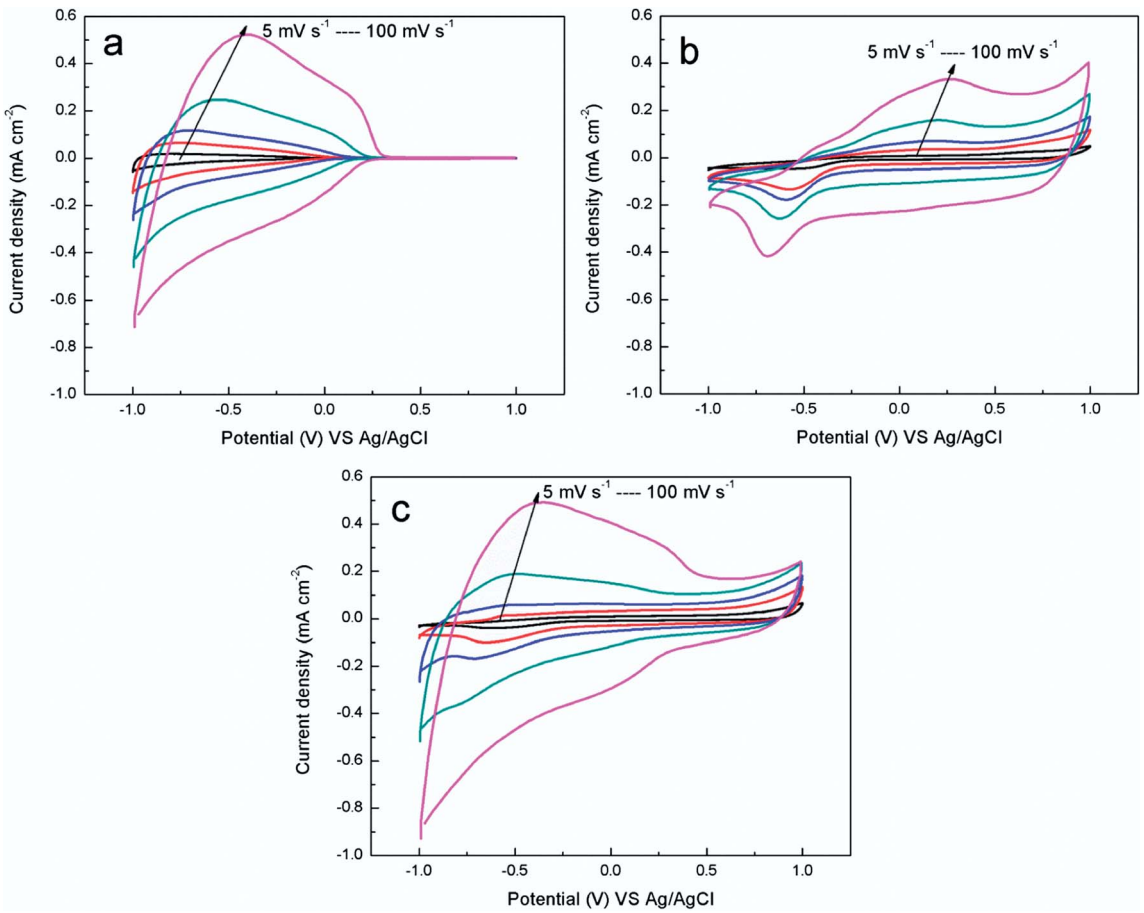


Fig. 6 Cyclic voltammetry plots of (a) $WO_3$, (b) PEDOT:PSS, (c) 5-bilayer hybrid thin films of the same thickness at scan rates of 5, 15, 25, 50, and 100 mV $s^{-1}$.

 This journal is © The Royal Society of Chemistry 2014

Published on 10 December 2013. Downloaded by Michigan State University on 20/01/2016 21:24:40.

optical contrast of the electrochromic films at the wavelength of interest ($\lambda_{int}$) can be expressed as the transmittance difference between the bleached and colored states at $\lambda_{int}$.[1] Fig. 7 shows UV-Vis transmission spectra of $WO_3$, PEDOT:PSS and 5 bilayer hybrid thin films under various potentials. The neat $WO_3$ thin film (Fig. 7a) exhibits an optical contrast of more than 25% in the wavelength range of 600 nm to 800 nm (*cf.* Fig. S5†). At $\lambda_{int}$ of 633 nm, where the human eye is most sensitive, an optical contrast of 29% is achieved.[31] Beyond 633 nm, the optical contrast of $WO_3$ increases slowly and reaches ~35% at 800 nm. The PEDOT:PSS thin film exhibits its maximum optical contrast of 32% at $\lambda_{int}$ of 600 nm (Fig. 7b) as there is an obvious absorption peak at 600 nm at its colored state. The UV-Vis spectrum of the hybrid thin film is obviously a combined spectrum of the two components (Fig. 7c). At negative potential −1.0 V, the hybrid thin film exhibits an optical transmittance curve similar to that of neat $WO_3$ in shape, but with significantly lower transmittance. Moreover, a broad absorption peak caused by PEDOT:PSS reduction is noticeable at a wavelength of about 600 nm, indicating the simultaneous reduction of both components. At positive potential +0.8 V, the transmittance of the hybrid film is generally in between those of $WO_3$ and PEDOT:PSS films, implying that both components are switched to their bleached state. Not only the two components can be simultaneously switched, the hybrid thin film also exhibits higher optical contrast than the corresponding $WO_3$ and PEDOT:PSS films in a wavelength range from 600 nm to 800 nm, and the hybrid

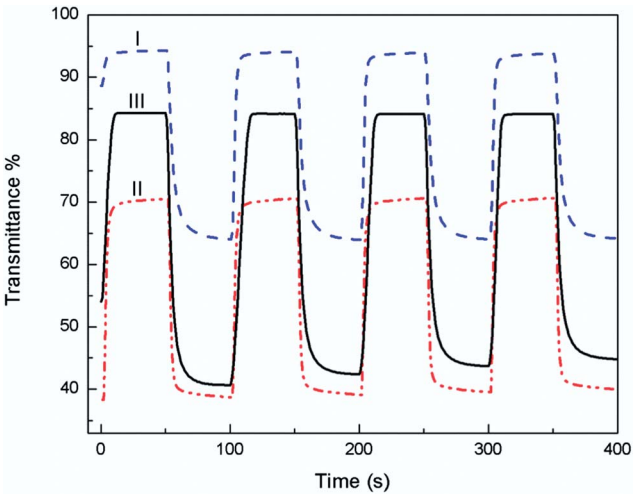


Fig. 8 Dynamic optical transmittance of the thin films of (I) $WO_3$ (blue dashed line), (II) PEDOT:PSS (red dash-dotted line), and (III) 5-bilayer hybrid (black solid line) under square wave potential oscillating between +0.8 V and −1.0 V at a time step of 50 s recorded at (I) 633, (II) 600 and (III) 645 nm, respectively.

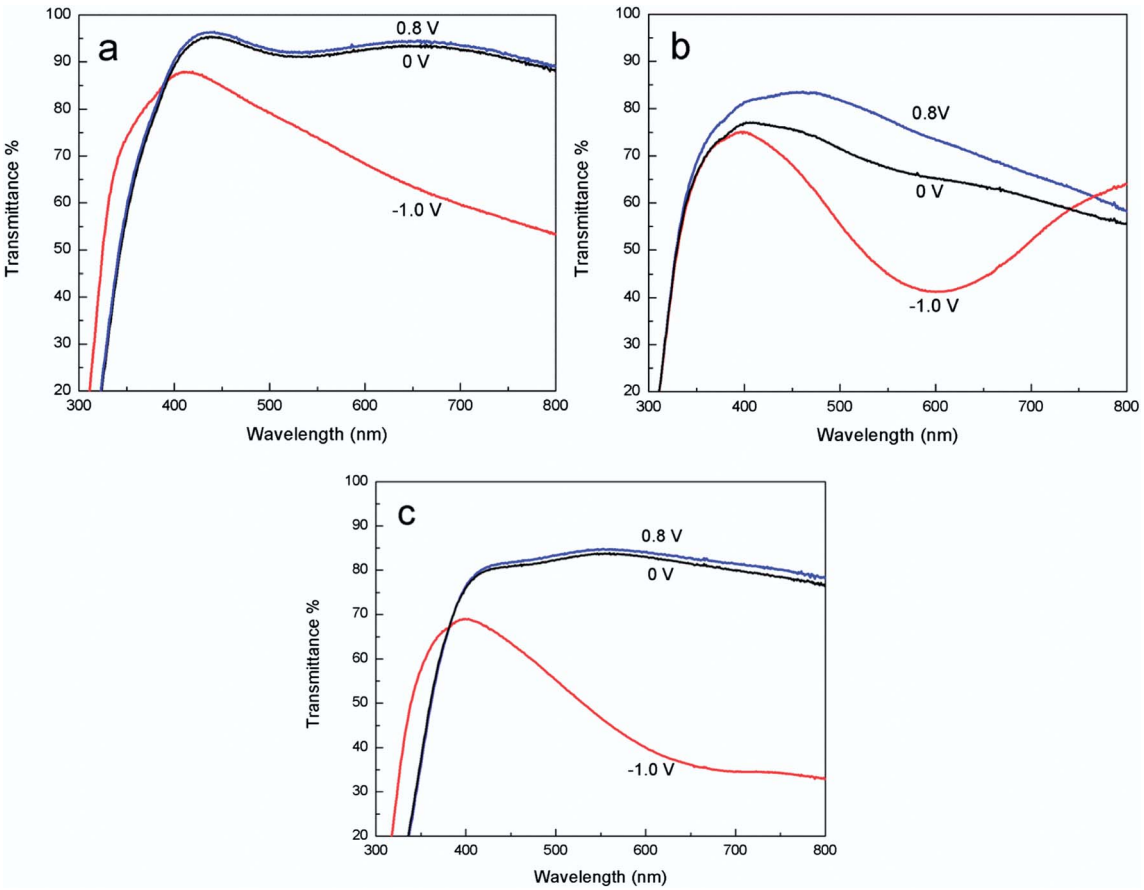


Fig. 7 UV-Vis optical transmittance spectra in the visible range of (a) $WO_3$, (b) PEDOT:PSS, and (c) 5-bilayer hybrid thin films under different potentials of 0.8, 0, and −1.0 V.

Published on 10 December 2013. Downloaded by Michigan State University on 20/01/2016 21:24:40.

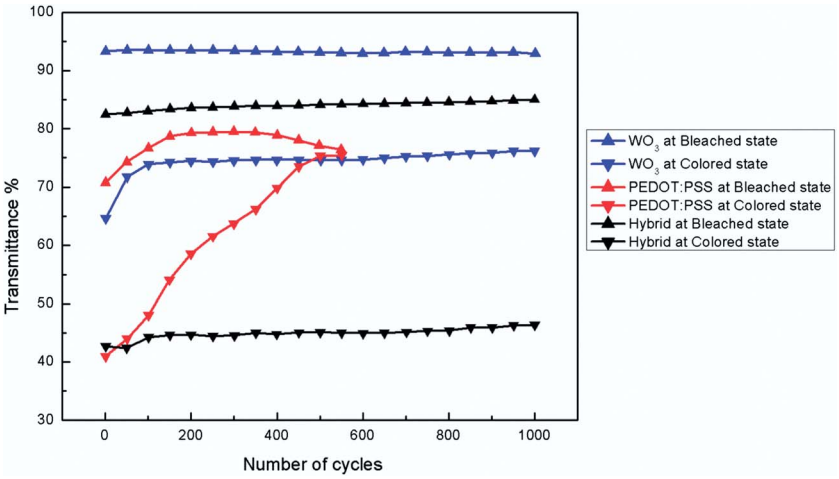


Fig. 9 Optical transmittance of $WO_3$, PEDOT:PSS, and 5-bilayer hybrid thin films at their colored and bleached states as a function of switching cycles. The transmittance was measured at $\lambda_{max}$ of each film, respectively.

film maintains a nearly constant contrast beyond 645 nm (*cf.* Fig. S5†). The enhanced optical contrast may again be attributed to the easier charge insertion/extraction into/from $WO_3$ caused by its interactions with PEDOT:PSS. Therefore, more $WO_3$ units can be effectively switched in the hybrid film, leading to higher optical contrast.

The transmittance of the three electrochromic thin films at their $\lambda_{int}$ under square-wave potential oscillating between +0.8 and −1.0 V at a time interval of 50 s is illustrated in Fig. 8. The dynamic contrast of the hybrid film is about 45%, which is again much higher than that of neat $WO_3$ or PEDOT:PSS films. From the plot, the transmittance of the hybrid is in between those of the $WO_3$ and PEDOT:PSS films in either bleached or colored states. It reconfirms that both components contribute to the bleaching and coloration process. The coloration efficiency of the hybrid film is also in between those of $WO_3$ and PEDOT:PSS films (*cf.* Fig. S6†). Regarding the switching kinetics, the PEDOT:PSS, $WO_3$ and hybrid films exhibit similar fast bleaching behaviour, whereas their coloration is slower. The coloration time for a neat $WO_3$ film (10 s) is significantly longer than that of a neat PEDOT:PSS film (5 s) presumably owing to the slower ion diffusion in $WO_3$. The coloration time of the hybrid film is 8 s, implying that the PEDOT:PSS surrounding $WO_3$ domains could facilitate the charge transfer process of $WO_3$ in the hybrid film.

To investigate the electrochemical stability of the hybrid film, the transmittance at bleached and colored states of the $WO_3$, PEDOT:PSS and hybrid thin films was measured under a square wave potential oscillating between +0.8 and −1.0 V for 1000 cycles (Fig. 9). In the first 100 cycles, the optical contrast of the $WO_3$ film decreases dramatically from 29% to about 20%. This is likely to be caused by the presence of structural defects in as-deposited hybrid films, which provide many interstitial sites initially.[32] Such defect sites may be consumed in the redox switching, since the $Li^+$ ion could be entrapped in these interstitial sites, causing the initial reduction in contrast. It then maintains most of the optical contrast in the following cycles. For the PEDOT:PSS thin film, the optical contrast continuously deteriorates and it completely loses its electrochromic activity after about 500 cycles as a consequence of the over-oxidation of PEDOT:PSS. The hybrid thin film exhibits remarkably improved stability, retaining 97% of its original contrast after 1000 cycles. The enhanced stability of the hybrid can be attributed to two major factors: (1) PEDOT:PSS may enter the defect sites in the $WO_3$ lattice, as suggested by the XPS result presented in Fig. 4a, acting as a buffer layer to prevent the surface-defect-induced anodic dissolution and cyclic erosion in the first 100 cycles; (2) the surface functional groups of $WO_3$ may act as dopants to prevent the over-oxidation of PEDOT:PSS.[13,28]

## 4. Conclusions

In summary, multilayer hybrid thin films consisting of PEDOT:PSS and $WO_3$ were readily prepared using a one-pot sequential electrochemical deposition method. The method provides a simple and efficient way to produce hybrid thin films with large interfacial area. Moreover, the morphology of the hybrid thin films can be easily manipulated by adjusting the deposition parameters, such as deposition time or potentials. Thus, the interactions between the two phases can be well controlled to optimize the electrochromic performance of the thin films. In the hybrid thin films, PEDOT:PSS and $WO_3$ can be simultaneously switched to coloured/bleached states, exhibiting significantly improved optical contrast and stability compared with neat PEDOT:PSS or $WO_3$ films.

## Acknowledgements

This work was supported by National Research Foundation (NRF), Singapore under Campus for Research Excellence And Technological Enterprise (CREATE), and Science and Engineering Research Council of the Agency for Science, Technology and Research (A*STAR) and Ministry of National Development, Singapore under Grant 132 176 0013.

 This journal is © The Royal Society of Chemistry 2014

Published on 10 December 2013. Downloaded by Michigan State University on 20/01/2016 21:24:40.

## References

1 V. K. Thakur, G. Ding, J. Ma, P. S. Lee and X. Lu, *Adv. Mater.*, 2012, **24**, 4071–4096.
2 D. T. Gillaspie, R. C. Tenent and A. C. Dillon, *J. Mater. Chem.*, 2010, **20**, 9585–9592.
3 P. M. Beaujuge and J. R. Reynolds, *Chem. Rev.*, 2010, **110**, 268–320.
4 S. Y. Park, J. M. Lee, C. Noh and S. U. Son, *J. Mater. Chem.*, 2009, **19**, 7959–7964.
5 C.-L. Lin, C.-C. Lee and K.-C. Ho, *J. Electroanal. Chem.*, 2002, **524–525**, 81–89.
6 S. Vogel and R. Holze, *Electrochim. Acta*, 2005, **50**, 1587–1595.
7 S. Xiong, S. L. Phua, B. S. Dunn, J. Ma and X. Lu, *Chem. Mater.*, 2009, **22**, 255–260.
8 J. Zhang, J.-P. Tu, D. Zhang, Y.-Q. Qiao, X.-H. Xia, X.-L. Wang and C.-D. Gu, *J. Mater. Chem.*, 2011, **21**, 17316–17324.
9 G. A. Niklasson and C. G. Granqvist, *J. Mater. Chem.*, 2007, **17**, 127–156.
10 R. Kirchgeorg, S. Berger and P. Schmuki, *Chem. Commun.*, 2011, **47**, 1000–1002.
11 G. Gunbas and L. Toppare, *Chem. Commun.*, 2012, **48**, 1083–1101.
12 S. Liu, L. Xu, F. Li, B. Xu and Z. Sun, *J. Mater. Chem.*, 2011, **21**, 1946–1952.
13 M. Deepa, A. K. Srivastava, K. N. Sood and A. V. Murugan, *J. Electrochem. Soc.*, 2008, **155**, D703–D710.
14 D. Szymanska, I. Rutkowska, L. Adamczyk, S. Zoladek and P. Kulesza, *J. Solid State Electrochem.*, 2010, **14**, 2049–2056.
15 L. Qin, J. Xu, B. Lu, Y. Lu, X. Duan and G. Nie, *J. Mater. Chem.*, 2012, **22**, 18345–18353.
16 D. S. Dalavi, R. S. Devan, R. A. Patil, R. S. Patil, Y.-R. Ma, S. B. Sadale, I. Kim, J.-H. Kim and P. S. Patil, *J. Mater. Chem. C*, 2013, **1**, 3722–3728.
17 S. H. Baeck, T. Jaramillo, G. D. Stucky and E. W. McFarland, *Nano Lett.*, 2002, **2**, 831–834.
18 Y. Lu, L. Liu, D. Mandler and P. S. Lee, *J. Mater. Chem. C*, 2013, **1**, 7380–7386.
19 P. Shen, N. Chi and K.-Y. Chan, *J. Mater. Chem.*, 2000, **10**, 697–700.
20 J. Qin, M. Cao, N. Li and C. Hu, *J. Mater. Chem.*, 2011, **21**, 17167–17174.
21 D. Alemu Mengistie, P.-C. Wang and C.-W. Chu, *J. Mater. Chem. A*, 2013, **1**, 9907–9915.
22 C. Li and T. Imae, *Macromolecules*, 2004, **37**, 2411–2416.
23 G. Wang, Y. Ling, H. Wang, X. Yang, C. Wang, J. Z. Zhang and Y. Li, *Energy Environ. Sci.*, 2012, **5**, 6180–6187.
24 S.-H. Lee, H. M. Cheong, C. E. Tracy, A. Mascarenhas, D. K. Benson and S. K. Deb, *Electrochim. Acta*, 1999, **44**, 3111–3115.
25 G. S. Kanner and D. P. Butt, *J. Phys. Chem. B*, 1998, **102**, 9501–9507.
26 A. P. Shpak, A. M. Korduban, M. M. Medvedskij and V. O. Kandyba, *J. Electron Spectrosc. Relat. Phenom.*, 2007, **156–158**, 172–175.
27 S.-I. Na, G. Wang, S.-S. Kim, T.-W. Kim, S.-H. Oh, B.-K. Yu, T. Lee and D.-Y. Kim, *J. Mater. Chem.*, 2009, **19**, 9045–9053.
28 L. Zhang, S. Xiong, J. Ma and X. Lu, *Sol. Energy Mater. Sol. Cells*, 2009, **93**, 625–629.
29 S. Xiong, P. Jia, K. Y. Mya, J. Ma, F. Boey and X. Lu, *Electrochim. Acta*, 2008, **53**, 3523–3530.
30 P. Jia, A. A. Argun, J. Xu, S. Xiong, J. Ma, P. T. Hammond and X. Lu, *Chem. Mater.*, 2009, **21**, 4434–4441.
31 S. S. Kalagi, S. S. Mali, D. S. Dalavi, A. I. Inamdar, H. Im and P. S. Patil, *Electrochim. Acta*, 2012, **85**, 501–508.
32 S. A. Agnihotry, R. Sharma, M. Kar and T. K. Saxena, *Sol. Energy Mater. Sol. Cells*, 2006, **90**, 15–24.